Transport and Communications Science Journal, Vol. 76, Issue 04 (05/2025), 541-555

Transport and Communications Science Journal

ONLINE DETERMINATION OF REFERENCE CURRENTS FOR WIDE-SPEED RANGE OPERATION OF IPMSM IN ELECTRIC VEHICLES USING THE NEWTON-RAPHSON METHOD

Thanh Lich Nguyen[1*], Thanh Loan Pham[2]

[1]University of Transport and Communications, No 3 Cau Giay Street, Hanoi, Vietnam

[2]Hanoi University of Mining and Geology, No 18 Vien Street, Hanoi, Vietnam

ARTICLE INFO

TYPE: Research Article
Received: 19/11/2024
Revised: 07/03/2025
Accepted: 10/05/2025
Published online: 15/05/2025
https://doi.org/10.47869/tcsj.76.4.8

[*] *Corresponding author*
Email: lichnt@utc.edu.vn

Abstract. The Interior Permanent Magnet Synchronous Motor (IPMSM) has been widely employed as a preferred choice for electric vehicle (EV) because of its advantageous characteristics such as high efficiency, high-power density, and a robust operation. This paper focuses on the control of an IPMSM for EV applications, with emphasis on smooth transitions over a wide speed range, including both normal and high-speed operating regions. A comprehensive review of state-of-the-art IPMSM control methods is provided, followed by fundamental machine principles. Over-modulation techniques are then presented to effectively manage the maximum voltage of the DC-link source, a critical aspect for EV powertrains. In order to control the machine over a wide-speed range, a flux-weakening method has to be adopted by combining the conventional space vector modulation (SVM) in the normal speed range and the voltage angle control in the high-speed regions. A key innovation of this study is the use of the Newton-Raphson method to determine the optimum operating point of the IPMSM, minimizing the stator current for a given torque demand. This optimization not only maximizes the torque capability over the entire speed range, but also enhances the dynamic performance of the system, which is essential for EV applications requiring rapid and precise response. The proposed control strategy combines SVM with overmodulation techniques, enabling seamless transitions between low- and high-speed regions. Simulation results are used to validate the effectiveness of the proposed control strategy, demonstrating stable and robust performance under varying speed and load torque conditions, highlighting its potential for applications in wide-speed-range IPMSM-based EV systems.

Keywords: Wide-speed range, IPMSM, Newton-Raphson method, Machine identification.

1. INTRODUCTION

Electrical drive systems play a critical role in modern transportation, including applications such as subways, buses, and, in particular, electric vehicles (EVs) and hybrid electric vehicles (HEVs) [1]-[8]. Among various motor technologies, the Interior Permanent Magnet Synchronous Motor (IPMSM) has been widely employed as a preferred choice for EVs due to its advantageous characteristics, including high efficiency and high-power density, and a robust operation over a wide-speed range. In addition, the IPMSM has advantages over its counterpart, the surface-mounted permanent magnet synchronous machine (SPMSM), in terms of overload capability and wide-speed range [9]-[10]. The IPMSM motor, illustrated in Figure 1, features a buried-magnet rotor with alternating magnet poles. Due to the smaller magnet pole area compared to the rotor surface, the no-load air gap flux density is lower than the flux density inside the magnets. The d-axis (direct axis) aligns with the rotor's magnetic field and passes through the embedded magnets, representing the direction of maximum magnetic flux. In contrast, the q-axis (quadrature axis) is perpendicular to the d-axis and passes through the rotor's iron core, allowing the q-axis armature flux to flow without crossing the magnets. As a result, the synchronous reactance in the d-axis is lower than in the q-axis. Additionally, the embedded magnets are well protected from centrifugal forces. Since the permanent magnets are enclosed within the rotor, the IPMSM can achieve high-speed operation, reaching up to twice the rated speed. This characteristic makes it particularly well-suited for EV applications, especially for highway driving.

Despite these advantages, driving an IPMSM at high speeds presents several challenges. The primary limitation is the finite voltage supplied by the inverter. In addition, field-weakening control is required at high speeds, and the control algorithm must be able to provide a smooth transition between the normal- and the high-speed ranges. In order to utilize the maximum voltage provided by the feeding inverter, over-modulation techniques are often employed for two-level inverters. The over-modulation method can extend the fundamental phase voltage from $U_{\mathrm{dc}}/\sqrt{3}$ to $2 \cdot U_{\mathrm{dc}}/\pi$ by injecting high-frequency components into the stator winding. In addition to its advantage, this approach introduces harmonics in the phase currents, requiring current feedback signals to filter out high-frequency noise to prevent unwanted interference with the control loop [11].

In the over-modulation mode, the voltage margin for the current control loop is small, hence the current controllers are easily saturated. This phenomenon affects the dynamics of the current control loop. Furthermore, the modulation index in the over-modulation must be compensated accurately to keep the fundamental phase voltage constant. A method as was proposed in [12] is used in this paper to control a two-level inverter in the whole range of the modulation index.

For normal-speed operation, the maximum torque per ampere (MTPA) strategy is commonly adopted to optimize performance. In contrast, in the high-speed range, flux-weakening control is employed, reducing the pole flux to increase the speed while maintaining to the maximum phase voltage constraint of $2U_{\mathrm{dc}}/\pi$. This allows the machine to operate efficiently in the constant power region. Several methods for flux-weakening control have been proposed, including current angle control, voltage angle control, and combined torque and flux control [13]-[15]. The most critical requirement of the flux-weakening algorithm is the ability to cooperate with the conventional MTPA to provide a smooth transition between the normal and the high-speed regions. Other important requirements of the flux-weakening algorithm are

to ensure high dynamics of the control system and to be easily integrated with the conventional space vector modulation method.

This paper presents an indirect voltage angle-based method for field-weakening control that is designed to integrate seamlessly with conventional IPMSM control schemes. The Newton-Raphson method is used to determine the optimum operating point online at each speed and torque, rather than using look-up tables. This approach offers adaptability to variations in machine parameters caused by magnetic saturation and temperature changes, ensuring robust and efficient control over a wide speed range.

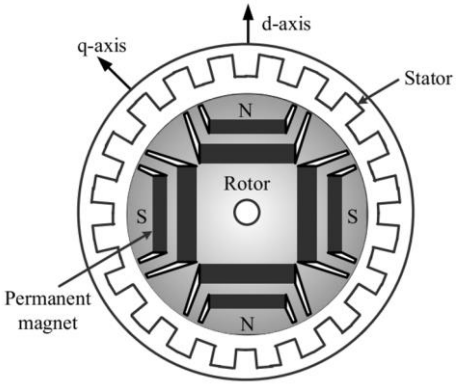

Figure 1. Structure of the IPMSM [16].

2. THEORETICAL FUNDAMENTAL OF IPMSMS

This section dedicates an overview on the mathematical description of IPMSMs and then the basic operation of the machine.

In the rotating d-q reference frame, the d-axis is aligned with the rotor flux, representing the flux-producing component, while the q-axis, which is perpendicular to the d-axis. This rotating d-q frame is commonly referred to as the rotor-fixed reference frame. The stator voltage equations in the d-q reference frame are expressed as follows:

$$\begin{cases} u_{\mathrm{d}} = R_{\mathrm{s}} \cdot i_{\mathrm{d}} + L_{\mathrm{d}} \cdot \dfrac{\mathrm{d}i_{\mathrm{d}}}{\mathrm{d}t} - \omega_{\mathrm{s}} \cdot L_{\mathrm{q}} \cdot i_{\mathrm{q}} \\ u_{\mathrm{q}} = R_{\mathrm{s}} \cdot i_{\mathrm{q}} + L_{\mathrm{q}} \cdot \dfrac{\mathrm{d}i_{\mathrm{q}}}{\mathrm{d}t} + \omega_{\mathrm{s}} \cdot L_{\mathrm{d}} \cdot i_{\mathrm{d}} + \omega_{\mathrm{s}} \cdot \lambda_{\mathrm{m}} \end{cases} \quad (1)$$

where u_{d}, u_{q} and i_{d}, i_{q} and L_{d}, L_{q} are the voltage, current and inductance with respect to the d- and q- axis, respectively; R_{s} is the stator resistance; ω_{s} is the synchronous speed and λ_{m} is the permanent magnet flux linkage.

The amplitude of the stator current is limited by a maximum value I_{sm} corresponding the thermal constrain of the machine.

$$I_{\mathrm{s}} = \sqrt{i_{\mathrm{d}}^2 + i_{\mathrm{q}}^2} \leq I_{\mathrm{sm}} \quad (2)$$

In the continuous working condition, I_{sm} can be set to equal to the nominal value I_{N}. Figure 2 shows numerous circles corresponding to the locus of the stator current with different magnitude values. If $I_{\mathrm{sm}} = I_{\mathrm{N}}$, then the operational points are located inside the circle named “IN Limit” as shown in Figure 2.

The electromagnetic torque (T_{e}) is given by:

$$T_e = \frac{3}{2} p \cdot \left(\lambda_m \cdot i_q + \left(L_d - L_q\right) \cdot i_q \cdot i_d\right) \quad (3)$$

where p is the number of pole pairs of the machine.

It can be seen that the electromagnetic torque is composed of two components: one is associated with the flux linkage of the permanent magnet, and the other is due to the reluctance of the machine. In the case of SPMSM, the direct- and quadrature-inductances, say L_d and L_q, respectively, are equal so the reluctance component is zero. Therefore, the maximum torque per ampere (MTPA) of the SPMSM is obtained by controlling $i_d^* = 0$, while the MTPA curve of the IPMSM (i_d^{MTPA}) is defined at each stator current amplitude I_s by the following equations [17].

$$i_d^{MTPA} = \frac{\lambda_m}{4 \cdot \left(L_d - L_q\right)} - \sqrt{\frac{\lambda_m^2}{16 \cdot \left(L_d - L_q\right)^2} + \frac{I_s^2}{2}} \quad (4)$$

$$i_q^{MTPA} = \sqrt{I_s^2 - \left(i_d^{MTPA}\right)^2} \quad (5)$$

In the steady state, the voltage equation for IPMSMs above the base speed is derived as follows:

$$(\lambda_m + L_d \cdot i_d)^2 + \left(L_q \cdot i_q\right)^2 = \left(\frac{U_{sm}}{\omega_s}\right)^2 \quad (6)$$

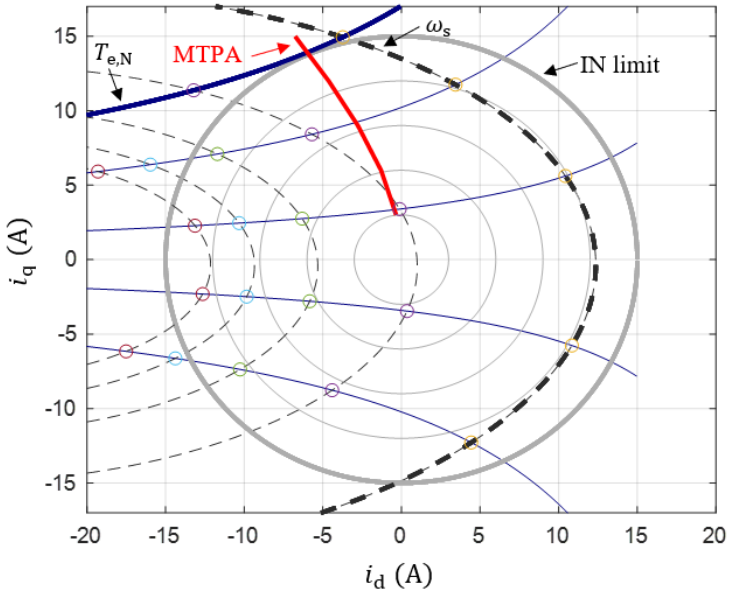

Figure 2. The locus of i_d, i_q for MTPA, current and voltage limit.

Where U_{sm} is the maximum output voltage of the feeding inverter. For the case of the 2-level inverter, $U_{sm} = U_{dc} \cdot 2/\pi$ is the maximum phase voltage and corresponds to the six-step mode of the inverter.

For a given electrical speed ω_s, the locus of $\left(i_d, i_q\right)$ satisfying (6) is a ellipse as shown in Figure 2. When ω_s increases, the ellipse shrinks. The machine can increase its operating speed until the corresponding ellipse does not intersect the limited circle.

There are some points to consider when controlling an IPMSM. The operating points always located inside the "IN limit" circle, as observed in Figure 2**.** When the machine operates below the base speed, the operating points are on the MTPA curve. As the electrical speed ω_s increases above

the base speed, the operating area becomes smaller. The intersection between the constant torque curves and the ellipses helps to determine the look-up table in the flux-weakening of the machine. Traditionally, this table can be pre-calculated based on the parameters of the machine, but they are parameters that depend on the motor's temperature and the stator current. The control algorithm should allow a smooth transition between the normal speed and the high speed region. The over-modulation algorithm must keep the fundamental in the actual modulated voltage equal to the reference value until the six-step mode is reached.

However, instead of using the look-up table to define the reference current, the paper proposes the Newton-Raphson method used to identify the optimal operating point of the machine, which includes the reference i_{d}^{*} and i_{q}^{*}. In the field weakening mode, the voltage angle is indirectly controlled by u_{d}^{*} and u_{q}^{*}. The current controller is saturated, which leads to the six-step operation mode, and the voltage angle is indirectly controlled by the reference voltage (even in the saturation condition).

As illustrated in Figure 3, the Reference Current Generator determines the reference currents i_{d}^{*} and i_{q}^{*} based on the motor speed ω_{s}. A Comparator evaluates the motor speed and selects the appropriate method accordingly. When the operating speed is below the nominal value, the MTPA method is employed to determine the reference current, and the conventional SVM technique is utilized [12]. Conversely, when the motor speed exceeds the rated speed, the Newton-Raphson Method is applied to compute the reference currents, ensuring efficient high-speed operation while maintaining system performance.

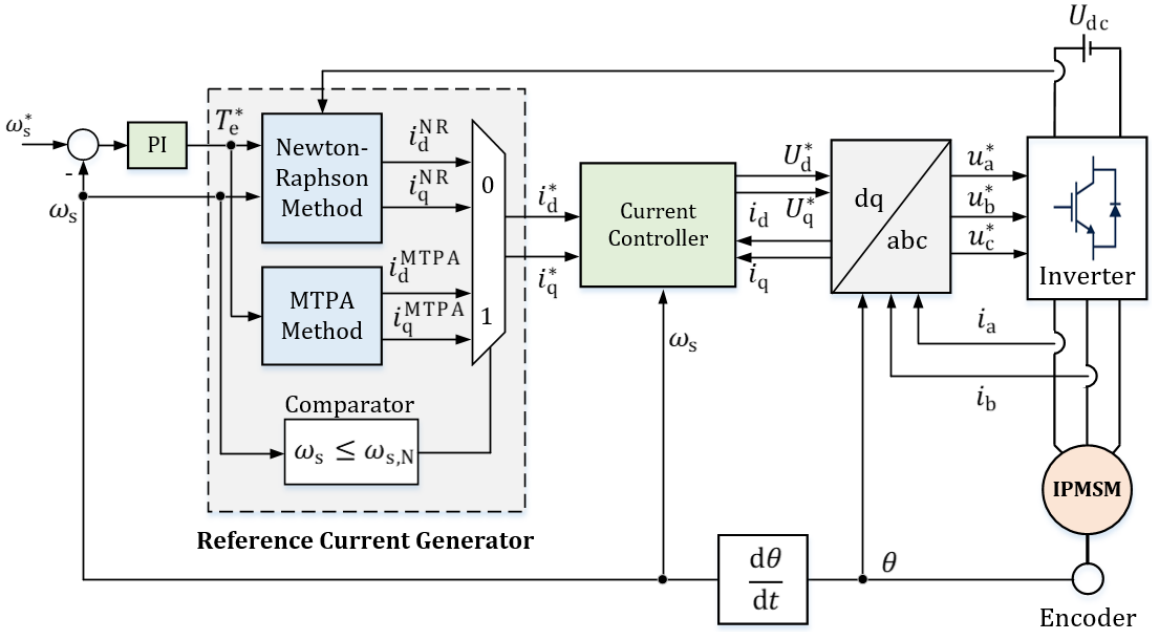

Figure 3. The block diagram of the proposed algorithm.

3. NEWTON-RAPHSON METHOD.

This section introduces the Newton-Raphson based method for finding the solution of non-linear equation system. Suppose that the nonlinear equation system is given in

$$\underline{f}(\underline{x}) = \begin{pmatrix} f_1(\underline{x}) \\ \dots \\ f_n(\underline{x}) \end{pmatrix} = \underline{0} \tag{7}$$

Where $\underline{x} = [x_1, \dots, x_n]^{\mathrm{T}}$ is the variable vector of the system of equations.
The Taylor's interpolation of $\underline{f}(\underline{x})$ in a vicinity of $\underline{x_0}$ is

$$\underline{f}(\underline{x}) = \underline{f}\left(\underline{x_0}\right) + \left.\frac{\partial \underline{f}}{\partial \underline{x}}\right|_{\underline{x_0}} \cdot \left(\underline{x} - \underline{x_0}\right) + O\left(\underline{x} - \underline{x_0}\right) \tag{8}$$

Where $G(\underline{x})$ is the gradient matrix vector given by

$$G(\underline{x}) = \frac{\partial \underline{f}}{\partial \underline{x}} = \begin{bmatrix} \frac{\partial f_1}{\partial x_1} \dots \dots \dots \frac{\partial f_1}{\partial x_n} \\ \dots \dots \dots \dots \dots \dots \\ \frac{\partial f_n}{\partial x_1} \dots \dots \dots \frac{\partial f_n}{\partial x_n} \end{bmatrix} \tag{9}$$

To make (8) in the form of a recursive approach, it can be written as follows:

$$\underline{0} = \underline{f}\left(\underline{x_k}\right) + G(\underline{x}) \cdot \left(\underline{x_{k+1}} - \underline{x_k}\right) \tag{10}$$

Or

$$\underline{x_{k+1}} = \underline{x_k} - G^{-1}(\underline{x}) \cdot \underline{f}\left(\underline{x_k}\right) \tag{11}$$

In terms of IPMSMs, the reference current components i_{d}^* and i_{q}^* are determined by the reference torque T_{ref} and the actual electrical speed ω_{s} in the flux-weakening mode.

$$\begin{cases} T_{\mathrm{ref}} = K_{\mathrm{mt}} \cdot i_{\mathrm{q}} + K_{\mathrm{rt}} \cdot i_{\mathrm{d}} \cdot i_{\mathrm{q}} \\ U_{\mathrm{sm}}^2 = \left(\dfrac{U_{\mathrm{dc}} \cdot 2}{\pi}\right)^2 = U_{\mathrm{d}}^2 + U_{\mathrm{q}}^2 \end{cases} \tag{12}$$

Where

$$K_{\mathrm{mt}} = \frac{3}{2} p \cdot \lambda_{\mathrm{m}};\ K_{\mathrm{rt}} = \frac{3}{2} p \cdot \left(L_{\mathrm{d}} - L_{\mathrm{q}}\right) \tag{13}$$

The Newton-Raphson method given in (11) for solving the equation system (12) demonstrates that the gradient matrix is in the size of 2x2, so its inversion can be easily computed. For the IPMSM motor, the nonlinear equation system is expressed as follows:

$$\underline{f}(\underline{x}) = \begin{pmatrix} f_1(\underline{x}) \\ f_2(\underline{x}) \end{pmatrix} = \begin{pmatrix} U_{\mathrm{sm}}^2 - U_{\mathrm{d}}^2 - U_{\mathrm{q}}^2 \\ T_{\mathrm{ref}} - K_{\mathrm{mt}} \cdot i_{\mathrm{q}} - K_{\mathrm{rt}} \cdot i_{\mathrm{d}} \cdot i_{\mathrm{q}} \end{pmatrix} = \underline{0} \tag{14}$$

Where $\underline{x} = \left[i_{\mathrm{d}}, i_{\mathrm{q}}\right]^{\mathrm{T}}$ is a transposed vector consisting of the components i_{d} and i_{q}. By substituting U_{d} and U_{q} from equation (1) into equation (14), assuming steady-state conditions $\mathrm{d}i_{\mathrm{d}}/\mathrm{d}t = \mathrm{d}i_{\mathrm{q}}/\mathrm{d}t = 0$, we obtain:

$$\begin{aligned} f_1(\underline{x}) &= U_{\mathrm{sm}}^2 - R_{\mathrm{s}}^2\left(i_{\mathrm{d}}^2 + i_{\mathrm{q}}^2\right) - \omega_{\mathrm{s}}^2\left(L_{\mathrm{d}}^2 \cdot i_{\mathrm{d}}^2 + L_{\mathrm{q}}^2 \cdot i_{\mathrm{q}}^2\right) - 2 \cdot R_{\mathrm{s}} \cdot \omega_{\mathrm{s}} \cdot i_{\mathrm{d}} \cdot i_{\mathrm{q}}\left(L_{\mathrm{d}} - L_{\mathrm{q}}\right) \\ &\quad - 2 \cdot \omega_{\mathrm{s}} \cdot \lambda_{\mathrm{m}}\left(R_{\mathrm{s}} \cdot i_{\mathrm{q}} + \omega_{\mathrm{s}} \cdot L_{\mathrm{d}} \cdot i_{\mathrm{d}}\right) - \omega_{\mathrm{s}}^2 \cdot \lambda_{\mathrm{m}}^2 \\ f_2(\underline{x}) &= T_{\mathrm{ref}} - K_{\mathrm{mt}} \cdot i_{\mathrm{q}} - K_{\mathrm{rt}} \cdot i_{\mathrm{d}} \cdot i_{\mathrm{q}} \end{aligned} \tag{15}$$

The gradient matrix vector is obtained as follows:

$$G(\underline{x}) = \frac{\partial \underline{f}}{\partial \underline{x}} = \begin{bmatrix} g_{11} & g_{12} \\ g_{21} & g_{22} \end{bmatrix} \tag{16}$$

where:

$$\begin{aligned} g_{11} &= \frac{\partial f_1}{\partial i_\mathrm{d}} = -2 \cdot \left(R_\mathrm{s}^2 + \omega_\mathrm{s}^2 \cdot L_\mathrm{d}^2\right) \cdot i_\mathrm{d} - 2 \cdot R_\mathrm{s} \cdot \omega_\mathrm{s}\left(L_\mathrm{d} - L_\mathrm{q}\right) \cdot i_\mathrm{q} - 2 \cdot \omega_\mathrm{s}^2 \cdot \lambda_\mathrm{m} \cdot L_\mathrm{d} \\ g_{12} &= \frac{\partial f_1}{\partial i_\mathrm{q}} = -2 \cdot \left(R_\mathrm{s}^2 + \omega_\mathrm{s}^2 \cdot L_\mathrm{q}^2\right) \cdot i_\mathrm{q} - 2 \cdot R_\mathrm{s} \cdot \omega_\mathrm{s}\left(L_\mathrm{d} - L_\mathrm{q}\right) \cdot i_\mathrm{d} - 2 \cdot \omega_\mathrm{s}^2 \cdot \lambda_\mathrm{m} \cdot R_\mathrm{s} \\ g_{21} &= \frac{\partial f_2}{\partial i_\mathrm{d}} = -K_\mathrm{mt} \cdot i_\mathrm{q} \\ g_{22} &= \frac{\partial f_2}{\partial i_\mathrm{q}} = -K_\mathrm{mt} - K_\mathrm{rt} \cdot i_\mathrm{d} \end{aligned} \tag{17}$$

The inverse of $G\left(\underline{x}\right)$ is given by:

$$G^{-1}\left(\underline{x}\right) = \frac{1}{\det(G)}\begin{bmatrix} g_{22} & -g_{12} \\ -g_{21} & g_{11} \end{bmatrix} \tag{18}$$

where

$$\begin{aligned} \det(G) = g_{11} \cdot g_{22} - g_{12} \cdot g_{21} \\ = \left[-2 \cdot \left(R_\mathrm{s}^2 + \omega_\mathrm{s}^2 \cdot L_\mathrm{d}^2\right) \cdot i_\mathrm{d} - 2 \cdot R_\mathrm{s} \cdot \omega_\mathrm{s}\left(L_\mathrm{d} - L_\mathrm{q}\right) \cdot i_\mathrm{q} - 2 \cdot \omega_\mathrm{s}^2\right. \\ \left. \cdot \lambda_\mathrm{m} \cdot L_\mathrm{d}\right] \cdot \left[-K_\mathrm{mt} - K_\mathrm{rt} \cdot i_\mathrm{d}\right] \\ - \left[-2 \cdot \left(R_\mathrm{s}^2 + \omega_\mathrm{s}^2 \cdot L_\mathrm{q}^2\right) \cdot i_\mathrm{q} - 2 \cdot R_\mathrm{s} \cdot \omega_\mathrm{s}\left(L_\mathrm{d} - L_\mathrm{q}\right) \cdot i_\mathrm{d} - 2 \cdot \omega_\mathrm{s}^2\right. \\ \left. \cdot \lambda_\mathrm{m} \cdot R_\mathrm{s}\right] \cdot \left[-K_\mathrm{mt} \cdot i_\mathrm{q}\right] \end{aligned} \tag{19}$$

Expanding the matrix multiplication from equation (11) with $\underline{x_k} = \left[i_{\mathrm{d},k}, \mathrm{i}_{\mathrm{q},k}\right]^\mathrm{T}$, we obtain:

$$\begin{bmatrix} i_{\mathrm{d},k+1} \\ i_{\mathrm{q},k+1} \end{bmatrix} = \begin{bmatrix} i_{\mathrm{d},k} \\ \mathrm{i}_{\mathrm{q},k} \end{bmatrix} - \frac{1}{\det(G)}\begin{bmatrix} g_{22} & -g_{12} \\ -g_{21} & g_{11} \end{bmatrix} \cdot \begin{bmatrix} f_1\left(i_{\mathrm{d},k}, i_{\mathrm{q},k}\right) \\ f_2\left(i_{\mathrm{d},k}, i_{\mathrm{q},k}\right) \end{bmatrix} \tag{20}$$

By substituting the expressions for g_{11}, g_{12}, g_{21} and g_{22}, the update equations are derived as follows:

$$\begin{aligned} i_{\mathrm{d},k+1} = i_{\mathrm{d},k} - \frac{1}{\det(G)} \\ \cdot \left[\left(-K_\mathrm{mt} - K_\mathrm{rt} \cdot i_{\mathrm{d},k}\right) \cdot f_1\left(i_{\mathrm{d},k}, i_{\mathrm{q},k}\right)\right. \\ + \left(2 \cdot \left(R_\mathrm{s}^2 + \omega_\mathrm{s}^2 \cdot L_\mathrm{q}^2\right) \cdot i_{\mathrm{q},k} + 2 \cdot R_\mathrm{s} \cdot \omega_\mathrm{s}\left(L_\mathrm{d} - L_\mathrm{q}\right) \cdot i_{\mathrm{d},k} + 2 \cdot \omega_\mathrm{s}^2\right. \\ \left.\left. \cdot \lambda_\mathrm{m} \cdot R_\mathrm{s}\right) \cdot f_2\left(i_{\mathrm{d},k}, \mathrm{i}_{\mathrm{q},k}\right)\right] \end{aligned} \tag{21}$$

$$\begin{aligned} i_{\mathrm{q},k+1} = i_{\mathrm{q},k} - \frac{1}{\det(G)} \\ \cdot \left[\left(K_\mathrm{mt} \cdot i_{\mathrm{q},k}\right) \cdot f_1\left(i_{\mathrm{d},k}, i_{\mathrm{q},k}\right)\right. \\ - \left(2 \cdot \left(R_\mathrm{s}^2 + \omega_\mathrm{s}^2 \cdot L_\mathrm{d}^2\right) \cdot i_{\mathrm{d},k} + 2 \cdot R_\mathrm{s} \cdot \omega_\mathrm{s}\left(L_\mathrm{d} - L_\mathrm{q}\right) \cdot i_{\mathrm{q},k} + 2 \cdot \omega_\mathrm{s}^2\right. \\ \left.\left. \cdot \lambda_\mathrm{m} \cdot L_\mathrm{d}\right) \cdot f_2\left(i_{\mathrm{d},k}, i_{\mathrm{q},k}\right)\right] \end{aligned} \tag{22}$$

These equations (21) and (22) describe the iterative update of $i_{\mathrm{d},k+1}$ and $i_{\mathrm{q},k+1}$ using the Newton-Raphson method. Note that at each iteration k, the values of $f_1, f_2, g_{11}, g_{12}, g_{21}$ and g_{22} are computed based on the current values $i_{\mathrm{d},k}$ and $i_{\mathrm{q},k}$ before performing the update. The operating point can be determined online without the need for a lookup table. Furthermore, the computational

complexity of the Newton-Raphson method remains manageable, making it suitable for implementation in any DSP microcontroller. The flow chart of the Newton-Raphson algorithm is demonstrated in Figure 4.

It is noted that the flux-weakening is triggered when the electrical speed is higher than a predefined value. Below this speed, the IPMSMs are controlled with an MTPA characteristic. In addition, the reference torque must be limited to ensure that the operating points are located inside an allowable region.

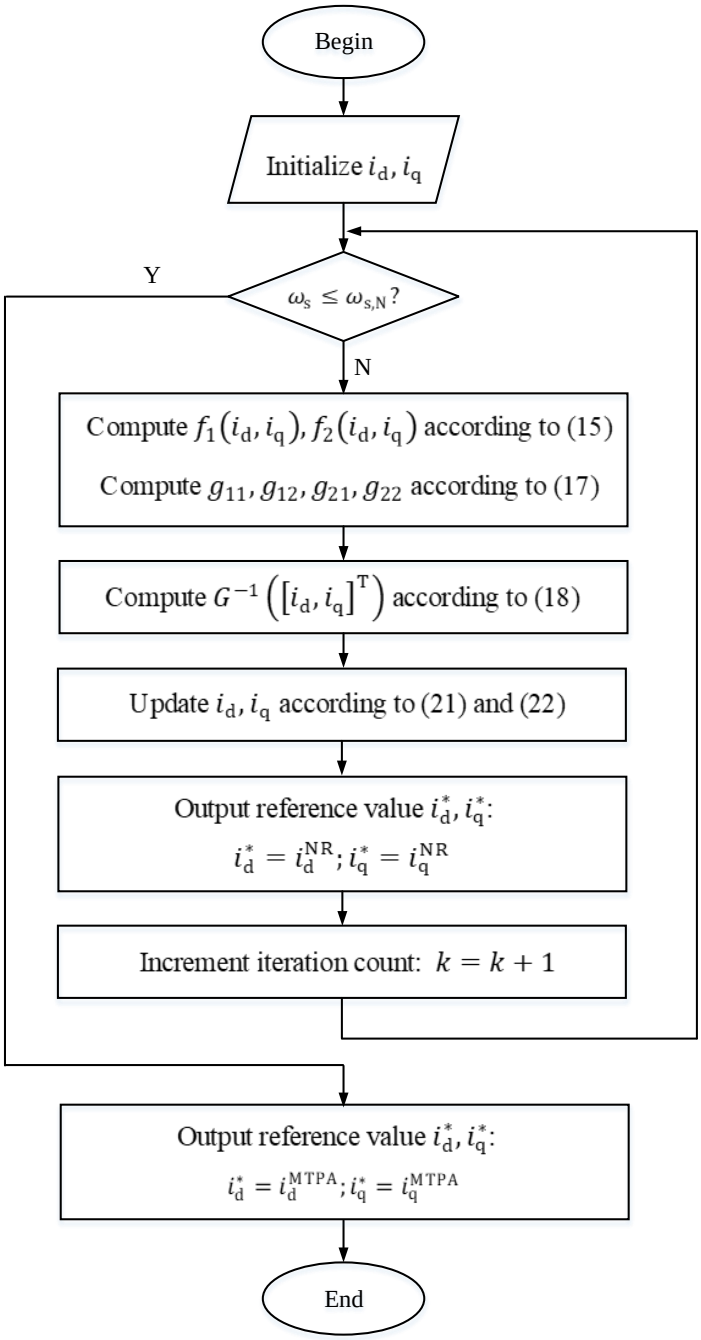

Figure 4. The flow chart of the Newton-Raphson algorithm.

4. PARAMETER IDENTIFICATION OF THE IPMSM IN THE SIX-STEP MODE

The output power of PWM-controlled AC motor drives is improved by increasing the inverter output voltage through overmodulation. In the six-step mode, the output voltage can be reached to a maximum possible value in continuously controllable fashion.

A comprehensive review of the state-of-the-art parameter estimation methods has been introduced in [18], where the machine's parameters can be identified by either online or offline techniques. Among the promising estimation methods, this work focuses on the recursive least mean square (RLMS), as it works in both low and high speed ranges and can be conducted in real time with affortable requirements on computational burden and stored memory of the microcontroller. In addition, RLMS can be operated against the noise [19]. In [19], the q-axis inductance and the voltage error are identified for the purpose of reducing the angle error in an encoderless control, since these two quantities have a significant effect on the precision of the angle observer algorithm. In this work, the flux linkage, d- and q-axis inductances and stator resistance are required to be updated to reconstruct the MTPA curve or to be used in the Newton-Raphson method to set the reference d- and q-axis current components.

There are several points to consider. First, in the six-step mode, the d- and q- currents are not seperately controlled, and current ripples are observed in both axes. As a result, the signal injection technique for the d and q inductance components may not be required as in the normal speed range as presented in [19]. Second, it is well known that the aforementioned four parameters are not estimated simultaneously, especially in the six-step mode when only the phase angle of the voltage is under control. The estimation of the four parameters can be carried out through the following sequential procedure: 1) set the rated or calculated values of the machine based on the datasheet or information obtained from the machine's nameplate; 2) determine the flux linkage of the machine; 3) estimate the d-axis and q-axis inductances; and 4) evaluate the stator resistance. Each step is executed sequentially with a processing time of 10 ms per step. This estimation process is supported by an analysis of the RLSM algorithm, focusing on aspects such as the error, convergence and dynamics [20]. Additionally, the stability margin of the speed control loop with respect to the identified parameters error must be considered to ensure the robust control performance. However, this aspect is beyond the scope of this paper and will be addressed in a future study.

5. OVERMODULATION METHOD

The modulation index (*MI*) is defined as the ratio between the magnitude of the reference voltage u_s^* and the maximum output voltage of a 2-level inverter corresponding to the six-step operation mode:

$$MI = \frac{|u_s^*|}{U_{dc} \cdot 2/\pi} \tag{1}$$

In the linear region of the space-vector modulation technique, the modulation index is limited by $MI = \left(\frac{1}{\sqrt{3}}\right)/(2/\pi) = 0.9069$. In the overmodulation region, the modulation index can reach 1 in the six-step operation. An overmodulation technique is required to cooperate with the conventional SVM to control the inverter in a whole modulation range. The technique as presented in [12] is adopted in this paper work. The reference voltage components in the direct and quadrature axes in the normal operationing point can be precisely modulated by the SVM technique, while in the field weakening region, the current controllers saturate, meaning that only voltage phase is indirectly controlled, while the amplitude is fixed to $U_{dc} \cdot 2/\pi$.

6. SIMULATION VERIFICATION

To validate the proposed control strategy, simulations were conducted with the main parameters of the motor are listed in Table 1. The simulation results are shown in Figure 5-Figure 10. Figure 5 illustrates the machine speed response regarding to the changes of reference speed and load torque. Initially, the reference speed increases from 0 to 1 p.u, then jumps to 2 p.u before settling at 1.5 p.u. The actual machine speed effectively tracks these changes, confirming the robustness of the control strategy. Furthermore, when the reference speed exceeds 1 p.u, the system enters the flux weakening region, where voltage constraints come into play.

Figure 6 presents the modulation index, which reflects how the inverter utilizes its voltage capability. When the system operates in the flux weakening region (above 1 p.u speed), the modulation index reaches 1, indicating that the current controllers are saturated, and the voltage is controlled primarily by its phase angle. This behavior ensures efficient utilization of the available DC bus voltage. As the speed increases, the reference torque is reduced, as shown in Figure 7, which is especially easy to observe in the time range from 0.2 s to 0.4 s. During this period, the reference torque is reduced to prevent excessive current demand while maintaining stable operation. The actual torque follows the reference closely, proving the effectiveness of the control strategy in tracking torque commands.

The reference currents i_{d}^{*} and i_{q}^{*} are changed accordingly, as shown in Figure 8 and Figure 9. Initially, i_{d}^{*} remains near zero but becomes negative when the system enters flux weakening mode to reduce the electromotive force (back EMF) and allow operation beyond the base speed. At low speeds, i_{q}^{*} is relatively high, ensuring sufficient torque. However, in the flux weakening region, i_{q}^{*} decreases to maintain the required torque while respecting the voltage and current limitations. It can be seen that both i_{d}^{*} and i_{q}^{*} closely follows the reference values, demonstrating the precise control of these currents.

Figure 10 shows the variation of the voltage angle, which plays a crucial role in controlling the stator voltage vector. In normal operation, the voltage angle follows a typical trajectory based on the current vector. However, in the flux weakening region, the modulation index is 1 as the current controllers are saturated, the voltage angle is adjusted to compensate for the reduced available voltage, ensuring stable operation at high speeds.

Table 1. Parameters of the motor.

Parameter	Symbol	Value	Unit
Rated torque	$T_{\mathrm{e,N}}$	2.5	Nm
Rated speed	n_{N}	3000	rpm
Maximum stator current	I_{sm}	15	A
Stator resistance	R_{s}	0.115	Ω
d- axis's inductance	L_{d}	3.56	mH
d- axis's inductance	L_{q}	7.25	mH
Pole pairs	p	1	
Moment of inertia	J	0.0006	Kg.m^2
Permanent magnet flux linkage	λ_{m}	0.0978	Vs
Switching frequency	f_{s}	10	kHz

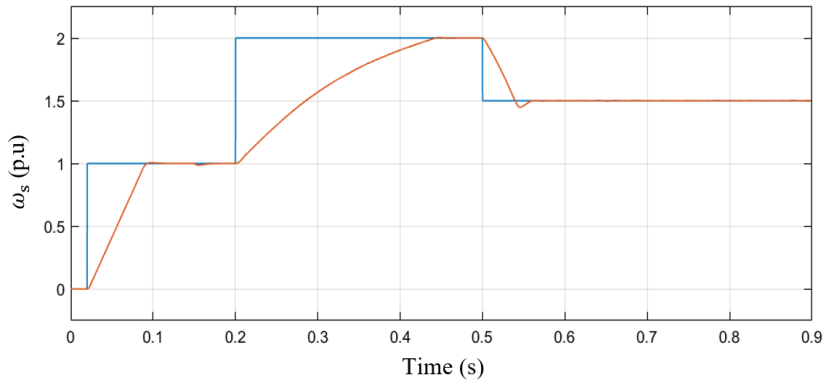

Figure 5. Speed response regarding to the changes of reference speed and load torque.

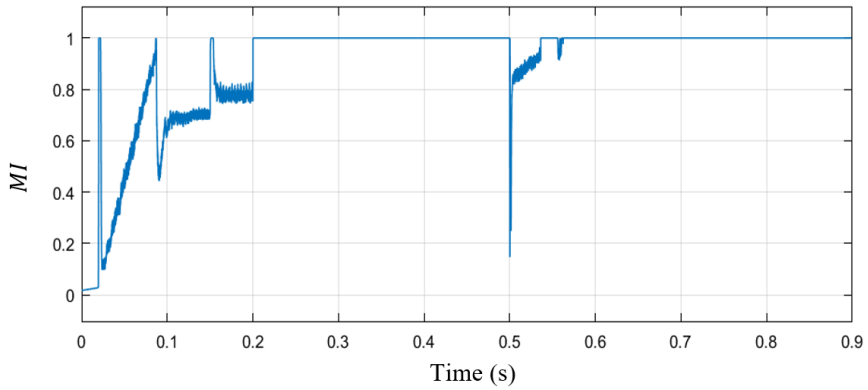

Figure 6. Modulation index.

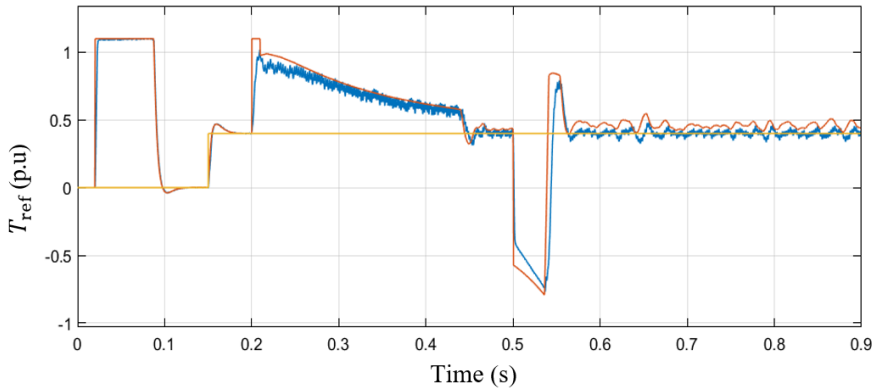

Figure 7. Load torque (in the orange), reference torque (in the red) and torque response (in the blue).

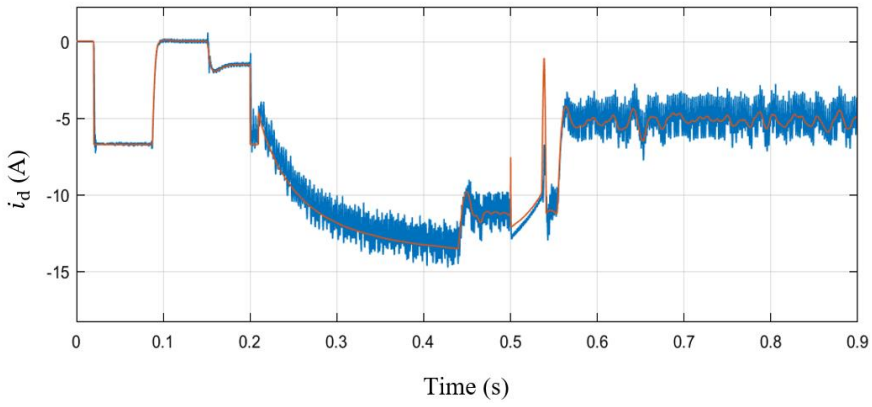

Figure 8. i_d reference (in the orange) and response (in the blue).

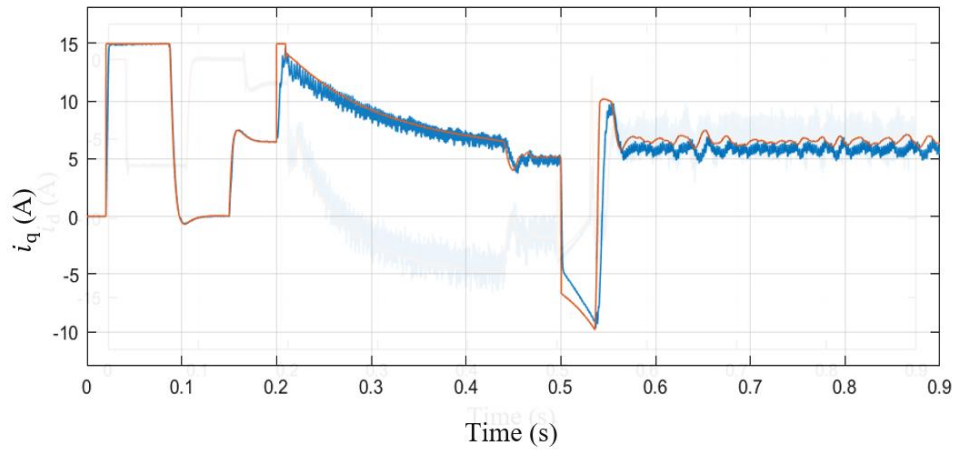

Figure 9. i_q reference (in the orange) and response (in the blue).

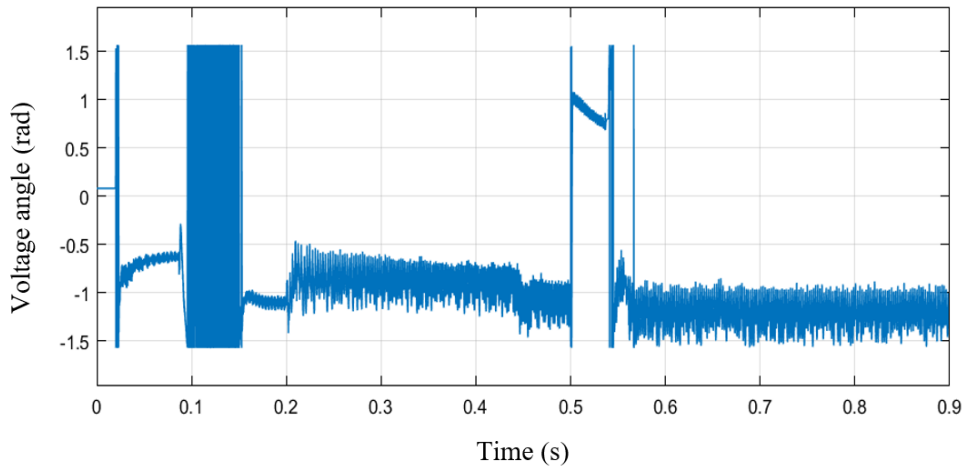

Figure 10. Voltage angle.

In practical operating conditions, key parameters of the IPMSM, such as direct-axis (L_d) and quadrature-axis (L_q) inductances, are not constant. These parameters vary due to multiple factors, including magnetic saturation, temperature rise in stator and rotor, and core losses. Such variations typically lead to a reduction in inductance values, resulting in reduced efficiency, unstable torque production, and challenges in high-speed operation. To evaluate the responsiveness of the Newton-Raphson control algorithm compared to the lookup table method under parameter variations, the inductance values L_d and L_q are reduced by half while maintaining the same speed and load response as in the simulation results shown in Figure 5-Figure 10. The corresponding simulation results for the modified inductance values are presented in Figure 11–Figure 14.

Traditional lookup table-based control strategies become ineffective in high-speed operation when the actual speed fails to track the reference value in the field-weakening region, as observed in Figure 11 between 0.2s and 0.5s. This limitation arises because the lookup table method relies on fixed, precomputed values of L_d and L_q, which become inaccurate under parameter variations. Consequently, incorrect reference currents are generated, leading to degraded performance, particularly in flux-weakening regions at high speeds.

In contrast, the Newton-Raphson method offers a significant advantage by determining machine parameters online, enabling real-time adaptation to parameter variations. This capability ensures stable and efficient operation across a wide speed range. As observed in Figure 11, the Newton-

Raphson method obtains faster and more precise reference speed tracking, whereas the lookup table method exhibits slower response and noticeable deviations during speed transitions.

The dynamics of the system are also influenced by the reference torque, which directly influences performance of the machine. As demonstrated in Figure 12, the actual torque more closely tracks the reference value when using the Newton-Raphson method, indicating its effectiveness in maximizing torque generation. This improvement is achieved due to the accurate real-time computation of i_d and i_q currents, as illustrated in Figure 13 and Figure 14, which are dynamically adjusted by the Newton-Raphson-based control algorithm.

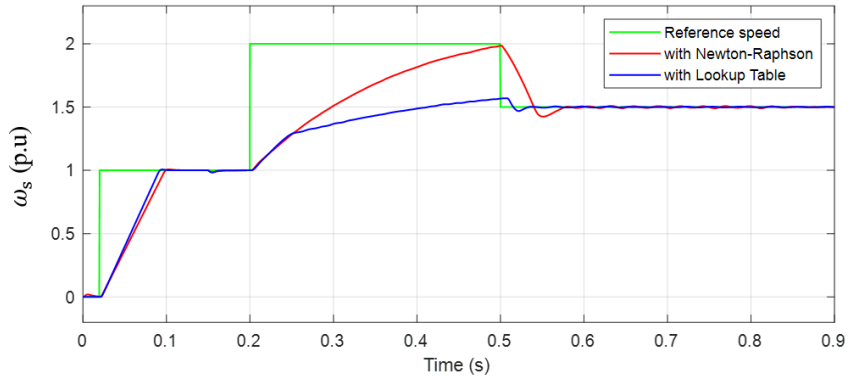

Figure 11. Speed response regarding to the changes of reference speed and load torque with and without Newton-Raphsoon Method.

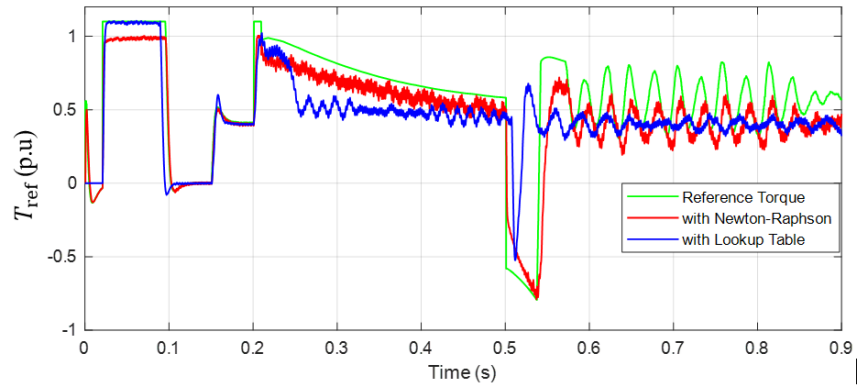

Figure 12. Torque response with and without Newton-Raphsoon Method.

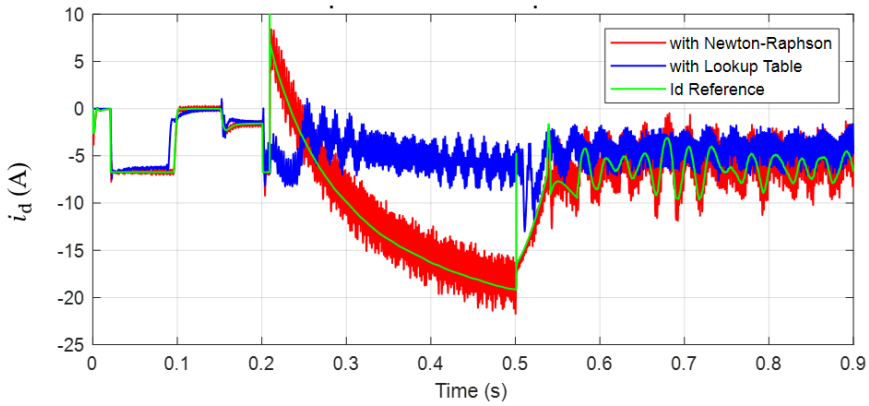

Figure 13. Direct current response (i_d) with and without Newton-Raphsoon Method.

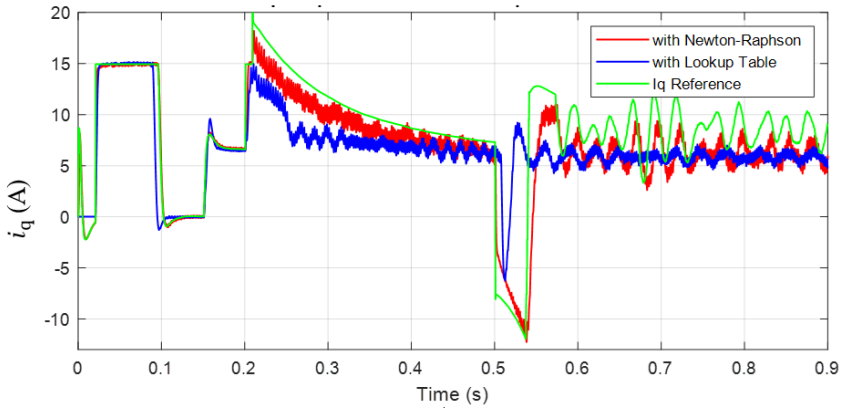

Figure 14. Quadrature current response (i_q) with and without Newton-Raphsoon Method.

7. CONCLUSIONS AND OUTLOOK

The proposed control strategy has demonstrated consistent and reliable performance in various scenarios involving changes in speed reference and load torque, demonstrating its suitability for EV applications. The seamless integration of overmodulation techniques with conventional SVM enables effective control, even under challenging conditions. In the flux-weakening mode, the stator voltage is controlled by the load angle, yet the system remains stable and provides a smooth transition between the low and high speed regions. While direct and quadrature currents are not separately controlled in this mode, the control strategy maintains robust torque regulation. Simulation results confirm the effectiveness of the proposed algorithms and illustrate their potential for wide-speed-range operation in EV systems. Although the Newton-Raphson method provides precise operating points and enhances system stability by accurately identifying machine parameters, it also has some limitations. Compared to look-up table methods, it requires higher computational time due to iterative calculations. Additionally, in high-speed flux-weakening mode, the system equations become highly nonlinear, which may increase the number of iterations needed for convergence or, in extreme cases, lead to convergence failure.

There are some prospects regarding this work that should be investigated in the future. Firstly, the Newton-Raphson method requires precise machine parameter identification, which could be achieved by signal injection at low speeds and recursive least square techniques at high speeds. (overmodulation). Secondly, the real-time reconstruction of MTPA trajectories through online parameter identification offers the opportunity to further improve efficiency and adaptability in dynamic EV environments.

REFERENCES

[1]. J. Fang, C. Heising, V. Staudt, A. Steimel, Permanent-magnet synchronous machine model for urban transport applications, Proc. 12th Int. Conf. Optim. Electr. Electron. Equip., (2010) 358-363. https://doi.org/10.1109/OPTIM.2010.5510539

[2]. P. B. Reddy, A. M. El-Refaie, K. K. Huh, J. K. Tangudu, T. M. Jahns, Comparison of interior and surface PM machines equipped with fractional-slot concentrated windings for hybrid traction applications, IEEE Trans. Energy Convers., 27 (2012) 593-602. https://doi.org/10.1109/TEC.2012.2195316

[3]. W. Wang, M. Cheng, B. Zhang, Y. Zhu, S. Ding, A fault-tolerant permanent-magnet traction module for subway applications, IEEE Trans. Power Electron., 29 (2014) 1646-1658.

https://doi.org/10.1109/TPEL.2013.2266377
[4]. K. C. Kim, A novel calculation method on the current information of vector inverter for interior permanent magnet synchronous motor for electric vehicle, IEEE Trans. Mag., 50 (2014) 829-832. https://doi.org/10.1109/TMAG.2013.2279555
[5]. M. S. Lim, S.-H. Chai, J.-P. Hong, Design of saliency-based sensorless-controlled IPMSM with concentrated winding for EV traction, IEEE Trans. Magn., 52 (2016). https://doi.org/10.1109/TMAG.2015.2474123
[6]. H. C. Jung, G.-J. Park, D.-J. Kim, S.-Y. Jung, Optimal design and validation of IPMSM for maximum efficiency distribution compatible to energy consumption areas of HD-EV, IEEE Trans. Magn., 53 (2017). https://doi.org/10.1109/CEFC.2016.7816180
[7]. S. C. Carpiuc, Rotor temperature detection in permanent magnet synchronous machine-based automotive electric traction drives, IEEE Trans. Power Electron., 32 (2017) 2090-2097. https://doi.org/10.1109/TPEL.2016.2567238
[8]. J. M. Mun, G.-J. Park, S. Seo, D.-W. Kim, Y.-J. Kim, S.-Y. Jung, Design characteristics of IPMSM with wide constant power speed range for EV traction, IEEE Trans. Magn., 53 (2017). https://doi.org/10.1109/TMAG.2017.2664859
[9]. G. Pellegrino, A. Vagati, P. Guglielmi, B. Boazzo, Performance comparison between surface-mounted and interior PM motor drives for electric vehicle application, IEEE Trans. Ind. Electron., 59 (2012) 803-811. https://doi.org/10.1109/TIE.2011.2151825
[10]. A. Vagati, G. Pellegrino and P. Guglielmi, Comparison between SPM and IPM motor drives for EV application, Proc. XIX Int. Conf. ICEM, (2010) 1-6. https://doi.org/10.1109/ICELMACH.2010.5607911
[11]. J. Holtz, W. Lotzkat, A. M. Khambadkone, On continuous control of PWM inverters in the overmodulation range including the six-step mode, IEEE Trans. Power Electron., 8 (1993) 546–553. https://doi.org/10.1109/63.261026
[12]. Dong-Choon Lee, G-Myoung Lee, A novel overmodulation technique for space-vector PWM inverters, IEEE Trans. Power Electron., 13 (1998) 1144–1151. https://doi.org/10.1109/63.728341
[13]. T. M. Jahns, Flux-Weakening Regime Operation of an Interior Permanent-Magnet Synchronous Motor Drive, IEEE Trans. Ind. Appl., 23 (1987) 681–689. https://doi.org/10.1109/TIA.1987.4504966
[14]. T. Miyajima, H. Fujimoto, M. Fujitsuna, A Precise Model-Based Design of Voltage Phase Controller for IPMSM, IEEE Trans. Power Electron., 28 (2013) 5655–5664. https://doi.org/10.1109/TPEL.2013.2259262
[15]. S. Bolognani, S. Calligaro, R. Petrella, F. Pogni, Flux-weakening in IPM motor drives: Comparison of state-of-art algorithms and a novel proposal for controller design, Proceedings of the 2011 14th European Conference on Power Electronics and Applications, (2011) 1-11.
[16]. L. Tian-Hua, Maximum efficiency control and predictive-speed controller design for interior permanent magnet synchronous motor drive systems, Frontiers in Electronics., 3(2022) https://doi.org/10.3389/felec.2022.904976
[17]. L. Qinghua, Analysis, design and control of permanent magnet synchronous motors for wide-speed operation, PhD Thesis, 2005. Accessed: 2021. [Online]. Available: https://scholarbank.nus.edu.sg/handle/10635/15011
[18]. T. Plazenet, T. Boileau, C. Caironi, B. Nahid-Mobarakeh, A Comprehensive Study on Shaft Voltages and Bearing Currents in Rotating Machines, IEEE Trans. Ind. Appl., 54 (2018) 3749 - 3759. https://doi.org/10.1109/TIA.2018.2818663
[19]. Y. Inoue, K. Yamada, S. Morimoto, M. Sanada, Effectiveness of Voltage Error Compensation and Parameter Identification for Model-Based Sensorless Control of IPMSM, IEEE Trans. Ind. Appl., 45 (2009) 213–221. https://doi.org/10.1109/TIA.2008.2009617
[20]. T. Söderström and L. Ljung, Theory and Practice of Recursive Identification. Cambridge, MA, USA: MIT Press, 1983.